JOURNAL OF PROPULSION AND POWER
Vol. 15, No. 5, September–October 1999

Individual Cylinder Model of a General Aviation Aircraft Engine

Gary Parker* and Giorgio Rizzoni†
Ohio State University, Columbus, Ohio 43210

A need exists for the improvement of general aviation (GA) aircraft piston engine performance through the use of advanced control strategies and diagnostic studies. The life cycle time associated with the development of these technologies is always a concern when working with a cost-restrictive budget. Approaches to technological improvements through trial-and-error experimentation can work against a budget due to cost and development time. With the advancements in the computational speed of computers, simulations have become increasingly popular in helping engineers solve problems more quickly through a better understanding of the problem and better preparation of design strategies prior to the experimental implementation stage. The aim of the present work is to develop an intermittent combustion aircraft engine simulation that can provide insight to the complex system behavior, aid in the development of control strategies, and aid in the development of diagnostic studies. The GA aircraft individual cylinder simulation is the first of its kind and it has many potential applications. Some potential applications may include idle speed control, fuel control, spark control, and engine sensor and actuator diagnostics.

Nomenclature

A_p = piston area
A_{prop} = fictitious propeller area
A_{run} = exhaust pipe mean cross-sectional area
A_{th} = open throttle area
A_{valve} = cylinder valve area
a = crank radius
a_{th} = ratio of throttle shaft diameter to throttle bore diameter
a_w = parameter for Wiebe function
B = damping coefficient for crankshaft dynamics
B_{piston} = piston diameter
C_D = propeller drag coefficient
$C_{D,\text{cyl}}$ = cylinder discharge coefficient
$C_{D,\text{th}}$ = throttle discharge coefficient
C_L = propeller lift coefficient
C_Q = propeller torque coefficient
c_1, c_2 = experimentally determined coefficients
D = throttle bore diameter
D_{prop} = propeller diameter
d = throttle shaft diameter
F_c = connecting rod force
F_p = piston head force generated from indicated pressure
F_t = force tangential to the crank radius
g = gravity constant
H = altitude
i = cylinder identification
J = inertia of reciprocating engine components including propeller
J_a = advance ratio of the propeller
L = stroke of piston
l = connecting rod length
M_{eq} = equivalent reciprocating mass
m = temperature/altitude constant
$m_{a,\text{cyl}}$ = mass of air in the cylinder
$m_{a,\text{ex}}$ = mass in exhaust manifold
$m_{a,m}$ = mass of air in the manifold
$\dot{m}_{a,\text{th}}$ = mass flow rate of air through the throttle
m_{fe} = mass of fuel entering the cylinder
m_{fi} = mass of fuel injected
m_{out} = mass out of exhaust manifold
m_{total} = total fuel in vapor and liquid phase
m_v = fuel vapor mass
m_w = parameter for Wiebe function
$m_{0,\text{cyl}}$ = initial mass in cylinder
N = engine speed
P_i = indicated pressure
P_m = manifold pressure
p = pressure at given altitude
p_{crank} = crankcase pressure
p_{cyl} = cylinder pressure
p_{ex} = exhaust manifold pressure
p_0 = sea-level pressure
Q_{app} = apparent heat release
Q_{ch} = gross heat release
Q_{ht} = heat transfer to through cylinder walls
Q_{lhv} = lower heating value
R = universal gas constant
R_L = length from exhaust valve to exhaust gas oxygen sensor
r_c = compression ratio
r_{eval} = radius of A_{prop}
r_{gy} = propeller radius of gyration
r_{prop} = propeller radius
T = temperature at given altitude
T_{cyl} = cylinder torque
T_{ex} = exhaust temperature
T_f = friction torque
T_i = indicated torque
T_{load} = load torque generated by propeller
T_m = manifold temperature
T_{oil} = oil temperature
T_{prop} = torque generated by propeller
T_r = reciprocating torque
T_0 = sea-level temperature
V = forward velocity of the aircraft
V_c = cylinder clearance volume
V_{cyl} = cylinder volume
V_d = cylinder displacement volume
V_m = manifold volume
V_T = total cylinder volume
X = mass fraction of fuel condensed on cylinder walls
x_b = mass fraction burned during combustion process
$\hat{x}_b$ = estimated mass fraction burned during combustion
$x_{b,\text{Total}}$ = total mass fraction burned

Received 26 May 1998; revision received 8 December 1998; accepted for publication 20 December 1998.

*Graduate Research Associate, Department of Mechanical Engineering, 206 West 18th Avenue; currently Engineer, Heavy Duty Applied Controls, Cummins Engine Company, Columbus, OH 43222.

†Associate Professor, Department of Mechanical Engineering, 206 West 18th Avenue.

α = propeller angle of attack
β = propeller geometric pitch angle
β_c = angle referenced from the vertical to the connecting rod
γ = specific heat ratio
γ_{prop} = $\beta - \alpha$
Δt = time delay for exhaust to reach exhaust gas oxygen sensor
$\Delta\theta$ = total combustion duration
ζ = T/T_0
η_v = volumetric efficiency
θ = crank-angle domain
θ_f = crank-angle location where Q_{app} decreases to zero
θ_I = crank-angle location after spark where Q_{app} is >0
θ_0 = start of combustion (spark)
λ = nondimensional term to describe propeller geometry
λ_{crank} = geometric description of crank radius to connecting rod length
μ = nondimensional term to describe propeller geometry
μ_f = engine oil viscosity
ξ = p/p_0
ρ = density at altitude H
τ = time constant for the fueling dynamics
ψ = throttle angle
ψ_0 = throttle angle at idle
ω = engine angular velocity

Introduction

CONSIDERABLE effort has recently gone into the development of a new generation of general aviation (GA) aircraft piston engines that will perform better than previous generations. Current GA engines use control technology that has not advanced since the World War II era. The pilot has to pay considerable attention in the cockpit by adjusting cumbersome multilever controls in an open-loop control fashion. Many of these open-loop control systems can become closed-loop systems with current technologies. Current research efforts will look to improve GA engine performance characteristics and reliability; reduce pilot work load, and hence, the human error factor; improve environmental safety through the reduction of aircraft noise and emissions; and reduce engine cost to increase affordability.

GA engine revitalization is now possible through the technological advancements of sensors and actuators used for control and diagnostics and through modern microcomputer technology. The automotive engine has already seen the successful implementation of actuators and sensors to improve engine performance. Electronic engine controllers (EEC) regulate subsystems such as fuel injection, spark advance, idle speed, and exhaust gas recirculation (EGR) to improve fuel consumption, to optimize engine torque output, to reject idle speed disturbances, and to improve emissions. The EEC will eliminate some pilot responsibility by closing the loop on various engine control systems. This may convert the multilever control to a single lever, much like an automobile driver uses a single pedal to demand power.

The initial step toward improving GA technology through the use of simulation had been taken through the development of a low-order nonlinear dynamic model.[1] This engine model, coupled to a variable-pitch propeller system, was used as an initial tool for the development of control and diagnostics strategies. The model implements a steady-state performance map to provide the end result of combustion, piston motion, valve timing, and exhaust. Results show that the model provides a reasonable representation of the propulsion system.

An extension of Ref. 1 is the development of a general-purpose simulation that will aid in the understanding of the transient behavior of the engine by capturing the individual cylinder dynamics.[2,3] Individual cylinder models for automotive engines have already been developed for the purpose of control and diagnostic studies.[4–10] Unlike the mean value model, these models consider the dynamic behavior of many engine subsystems on an individual cylinder basis. The dependence of this type of simulation on empirical maps is far less, e.g., than the model described in Ref. 1, and can be easily adapted for other engines by the simple modification of predefined engine-specific parameters.

Effects such as altitude changes and propeller torque generation that are mentioned in Refs. 1, 11, and 12 will be incorporated into the present model. The combination of the work of two simulations mentioned in the preceding text will form the basis for a general-purpose tool that may serve future research and development needs in the GA industry.

Individual Cylinder Model

A brief description of the individual cylinder model follows. The model used in this simulation is essentially a physical model. This model takes into account the dynamics of the various physical processes that must take place prior to the production of propulsive power. In simple terms one can think of the system as having air and fuel as inputs and torque at the propeller as the output. Air entering the engine through the air-intake nozzle passes over the throttle body. The flow of air through the throttle body is regulated by the throttle opening and is governed by the pressure differential across it. This air mixes with the fuel in the intake manifold. The fuel mass entering the intake manifold is governed by a continuous-flow system (open-loop control) based on the manifold pressure and the pilot commanded mixture setting. The air–fuel dynamics are an integral part of this model and are explained in some detail in the following sections. The air–fuel mixture that enters the cylinders is burned, releasing heat and generating indicated pressure. The model used for the combustion of fuel is a heat-release model that uses a Wiebe function to describe the burning rate of the fuel.[13] The indicated pressure is then converted to the indicated torque that drives the crankshaft, thus generating propulsive power. While the indicated torque accelerates the crankshaft there are other torques that work to impede this acceleration. These are the load, friction, and reciprocating torques. The net effect of these torques is seen through variations of the angular velocity of the crankshaft. The load torque for this application is the torque that the variable-pitch propeller exerts on the crankshaft. The friction torque is generated due to relative motion between the various reciprocating parts.

The products of combustion are exhausted out of the individual cylinder chambers into the exhaust manifold where, after some time delay, they reach the exhaust gas oxygen (EGO) or universal exhaust gas oxygen (UEGO) sensor. The EGO sensor is a binary sensor that outputs a high-voltage value for rich combustion (relative to the stoichiometric air–fuel ratio) or a low-voltage value for lean combustion. The UEGO sensor outputs a voltage proportional to the air–fuel ratio.

Figure 1 shows the basic system structure of the model, where T_{load} represents the load torque that the variable pitch propeller exerts on the crankshaft. Altitude effects cannot be seen explicitly in the

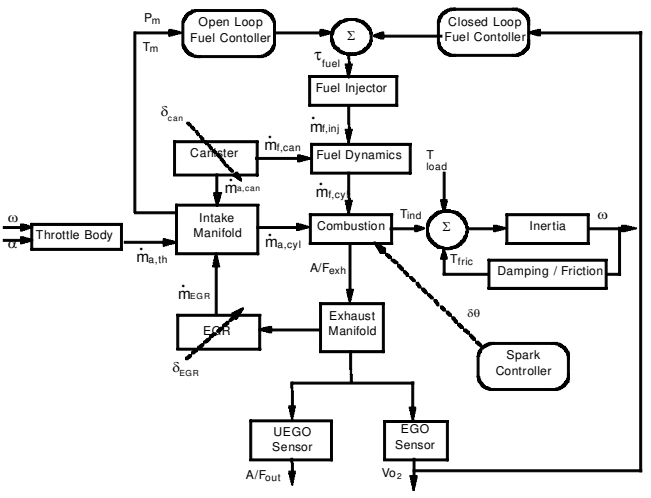

Fig. 1 Model structure.

system structure, but are implicit to the air dynamics. The altitude of the aircraft directly affects the mass of air flowing over the throttle in the intake manifold. Thus, the manifold pressure drops due to decreases in air density as the altitude increases. One can also see from the diagram that system blocks for fuel control, spark timing, EGR, and canister are included for the implementation of exhaust gas emissions control strategies.

The dynamics mentioned in the preceding discussion are described in detail in the sections that follow. Two additional features that are necessary for modeling a GA aircraft engine are a model for the change in air density with altitude and a model for the variable pitch propeller. These models are discussed in the following text.

Altitude Effects

The temperature relationship for the troposphere is given in Ref. 1 as

$$\zeta = 1 - 6.8729(10^{-6})H \tag{1}$$

ζ is a dimensionless quantity that tells how the temperature varies with respect to the sea-level temperature. In addition to temperature, the pressure variation with altitude was needed. The ideal gas law and the fundamental fluid equation of the pressure variation is derived in Ref. 12:

$$p = \rho RT, \qquad \frac{\mathrm{d}p}{\mathrm{d}h} = -\rho g \tag{2}$$

With these two equations, the following relationship can be defined for temperature and pressure:

$$(p/p_0) = (T/T_0)^{-g/mR} \tag{3}$$

In Ref. 1, (3) is expressed as

$$\xi = \zeta^{5.25581} \tag{4}$$

The legend in Fig. 2 indicates curves developed from two sources. The Parkinson equations were used in Ref. 1, and they were compared to the equations from Fox and McDonald.[12] The discrepancy is in the initial selection of sea-level temperature. However, because the discrepancy in densities is very small, the equations in Ref. 1 are used in the simulation for convenience.

Variable-Pitch Propeller Model

The method of the representative blade element model in Ref. 1 is used to model the load torque due to the propeller on the engine. This method assumes that torque can be approximated by a single blade element located at a distance r_{gy}. A fictitious propeller with radius r_{gy} and disk area A_{prop} is used. The model characterizes the basic torque dynamics without relying too much on the blade geometry. It does, however, rely on some empirical equations. These empirical equations are the lift and drag coefficients selected from Ref. 11. The lift coefficient C_L is dependent on the angle of attack α, which is the angle measured from a resultant velocity vector to the airfoil chord. The resultant velocity vector is the summation of the propeller rotational velocity $r\omega$ and the forward velocity of the aircraft V. The drag coefficient C_D is dependent on $\beta - \alpha$, which is the angle that is directly related to the forward velocity of the aircraft. The empirical coefficients are the following:

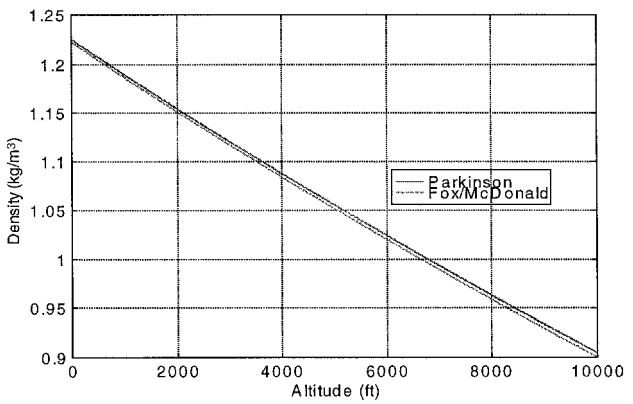

Fig. 2 Variation in density of air with altitude.

$$C_L = 0.1\alpha \tag{5}$$

$$C_D = 0.02 + 0.0002(\beta - \alpha)^2 \tag{6}$$

The geometric pitch angle of the propeller is described as β. It is measured from the plane of rotation to the airfoil chord. For a variable-pitch propeller system, the propeller blade has a hydraulic actuator/governor system that controls engine rpm to a steady-state value while changing the geometric blade pitch adjusts the load torque. For this simulation, the governor has not been modeled, thus the simulation user will have control over the pitch adjustment and the forward velocity of the aircraft. Given the forward velocity of the aircraft V, we can calculate the advance ratio J_a as

$$J_a = \frac{V}{ND_{\mathrm{prop}}} \tag{7}$$

The advance ratio can be described as the amount the plane advances for one rotation of the propeller. Knowing the advance ratio, the angle that is formed from the resultant velocity vector to the plane of rotation γ can be described by the following relationship:

$$\gamma_{\mathrm{prop}} = \tan^{-1}(J_a/\lambda) \tag{8}$$

where λ_g is a geometric description of the propeller blade. Another parameter involving the geometric description of the blade is μ. Both μ and λ can be described by the following relationships:

$$\mu = \frac{A_{\mathrm{prop}}}{2D_{\mathrm{prop}}^2} \tag{9}$$

$$\lambda = \frac{2\pi r_{\mathrm{eval}}}{D_{\mathrm{prop}}} \tag{10}$$

We are now in a position to express the torque that the propeller exerts on the crankshaft:

$$T_{\mathrm{prop}} = \rho N^2 D_{\mathrm{prop}}^5 C_Q \tag{11}$$

where C_Q is described by

$$C_Q = \frac{C_L \sin\gamma_{\mathrm{prop}} + C_D \cos\gamma_{\mathrm{prop}}}{\cos^2\gamma_{\mathrm{prop}}} \frac{\lambda^3 \mu}{2\pi} \tag{12}$$

Intake Air Dynamics Model

Figure 3 depicts a simplified representation of the intake air system of a GA engine. The system consists of a throttle body, a manifold, and individual cylinder runners. The air-dynamics model is based on the laws of continuity. The assumption made is that the manifold pressure is uniform at a given time instant. Continuity yields the following:

$$\frac{\mathrm{d}m_{a,m}}{\mathrm{d}t} = \dot{m}_{a,\mathrm{th}} - \sum_{i=1}^{\mathrm{numcyl}} \dot{m}_{a,\mathrm{cyl},i} \tag{13}$$

Equation (13) shows that the change in the mass of air in the manifold is dependent on the mass flow rate of air over the throttle plate and the mass flow rate entering the individual cylinders. The throttle position governs the area for the entering mass of air. However, as with any valve, friction and pressure differences also cause losses of energy. This results in less flow through the valve than the theoretical maximum. Additionally, fuel is sometimes injected in here so that the fuel and air can have some time to mix before being aspirated by the engine.

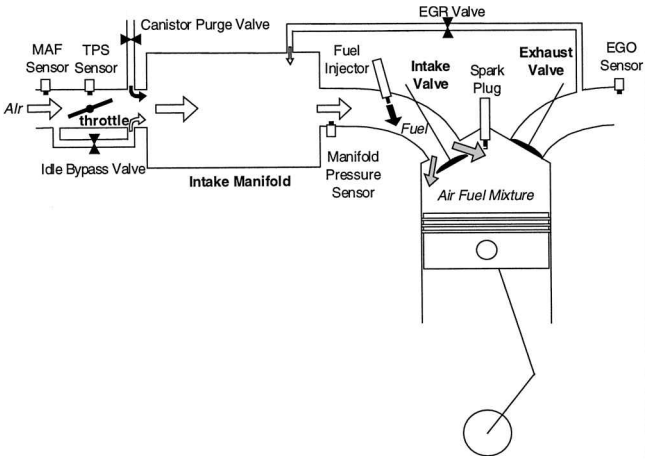

Fig. 3 Intake air system.

The throttle cross-sectional area is a function of geometry and of the throttle angle ψ.[13] The expression for the open throttle area A_{th} as a function of ψ is as follows:

$$\frac{4A_{\text{th}}}{\pi D^2} = \left(1 - \frac{\cos\psi}{\cos\psi_0}\right) + \frac{2}{\pi}\left[\frac{a_{\text{th}}}{\cos\psi}\left(\cos^2\psi - a_{\text{th}}^2\cos^2\psi_0\right)^{\frac{1}{2}} - \frac{\cos\psi}{\cos\psi_0}\sin^{-1}\left(\frac{a_{\text{th}}\cdot\cos\psi_0}{\cos\psi}\right) - a_{\text{th}}\left(1 - a_{\text{th}}^2\right)^{\frac{1}{2}} + \sin^{-1}a_{\text{th}}\right] \tag{14}$$

The variable a_{th} in Eq. (14) is the ratio of the throttle shaft diameter d to the throttle bore diameter D. Two sets of equations are modeled for two flow conditions. The first condition is for the case of pressure ratios across the throttle less than a critical value (unchoked flow). This condition is characterized by

$$p_m/p_0 > [2/(\gamma+1)]^{\gamma/(\gamma-1)} \tag{15}$$

for which the mass flow rate across the throttle plate is modeled as

$$\dot{m}_{a,\text{th}} = \frac{C_{D,\text{th}}A_{\text{th}}p_0}{\sqrt{RT_0}}\left(\frac{p_m}{p_0}\right)^{1/\gamma}\left\{\frac{2\gamma}{\gamma-1}\left[1 - \left(\frac{p_m}{p_0}\right)^{(\gamma-1)/\gamma}\right]\right\}^{\frac{1}{2}} \tag{16}$$

The choked condition is described by the following set of equations:

$$p_m/p_0 \le [2/(\gamma+1)]^{\gamma/(\gamma-1)} \tag{17}$$

$$\dot{m}_{a,\text{th}} = \frac{C_{D,\text{th}}A_{\text{th}}p_0}{\sqrt{RT_0}}\gamma^{\frac{1}{2}}\left(\frac{2}{\gamma+1}\right)^{(\gamma+1)/2(\gamma-1)} \tag{18}$$

The mass flow rate of air entering the cylinder is modeled similar to the mass flow rate of air across the throttle. For the unchoked condition

$$\dot{m}_{a,\text{cyl},i} = \frac{C_{D,\text{cyl}}A_{\text{valve}}p_m}{\sqrt{RT_m}}\left(\frac{p_{\text{cyl},i}}{p_m}\right)^{1/\gamma}\left\{\frac{2\gamma}{\gamma-1}\left[1 - \left(\frac{p_{\text{cyl},i}}{p_m}\right)^{(\gamma-1)/\gamma}\right]\right\}^{\frac{1}{2}} \tag{19}$$

Similarly, the choked condition is described as

$$\dot{m}_{a,\text{cyl},i} = \frac{C_{D,\text{cyl}}A_{\text{valve}}p_m}{\sqrt{RT_m}}\gamma^{\frac{1}{2}}\left(\frac{2}{\gamma+1}\right)^{(\gamma+1)/2(\gamma-1)} \tag{20}$$

The manifold pressure is generated from Eq. (20) by the ideal gas law:

$$p = mRT/V \tag{21}$$

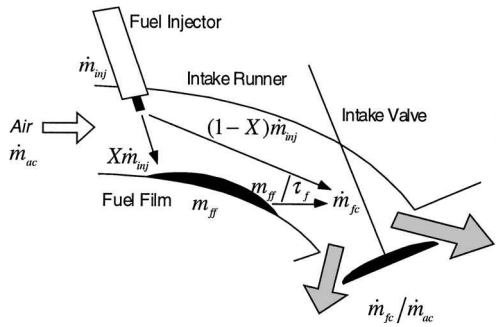

Fig. 4 Puddle phenomenon in fuel-injection subsystem.

Fuel Dynamics Model

Not all of the injected fuel enters the cylinder for combustion each cycle. For low engine temperatures, such as at engine startup, a portion of the fuel is deposited on the manifold walls in a liquid state, forming what is commonly known as the fuel puddle.[14] This phenomenon is qualitatively depicted in Fig. 4. Postinjection and prior to being aspirated for combustion, fuel coexists in three different phases: liquid fuel in the fuel puddle, finely atomized fuel as fuel mist, and evaporated fuel from the fuel puddle as fuel vapor.

The air–fuel mixture that enters the cylinder consists of the atomized mist and the evaporated fuel from the puddle. As the intake valve opens, this combination of fuel and air is drawn into the cylinder, and sometimes drops of liquid fuel will also drip into the cylinder.

For the IO-360, the fuel injection system is a continuous flow type. A nozzle is positioned at each intake runner that leads to each of the individual cylinder inlet valves. This is an open-loop system that allows better mixing of the air and fuel as opposed to a carburetor. The fuel dynamics equations are listed as follows:

$$m_v = (1-X)\dot{m}_{\text{fi}} \tag{22}$$

$$\dot{m}_{\text{fe}} = (1/\tau)(-\dot{m}_{\text{fe}} + X\dot{m}_{\text{fi}}) \tag{23}$$

$$\dot{m}_{\text{total}} = \dot{m}_v + \dot{m}_{\text{fe}} \tag{24}$$

Cylinder Pressure Development and Combustion Model

From Ref. 15, the mass flow into the cylinder during the intake stroke and the mass flow during the exhaust stroke are defined as

$$m_{\text{cyl}} = m_{0,\text{cyl}} + \int_{t,\text{IVO}}^{t,\text{IVC}}\dot{m}_{\text{cyl}}\,\mathrm{d}t = \frac{p_{0,\text{cyl}}M_{0,\text{cyl}}V_{0,\text{cyl}}}{\tilde{R}T_{0,\text{cyl}}} + \int_{t,\text{IVO}}^{t,\text{IVC}}\dot{m}_{\text{cyl}}\,\mathrm{d}t \tag{25}$$

$$m_{\text{cyl}} = m_{0,\text{cyl}} - \int_{t,\text{EVO}}^{t,\text{EVC}}\dot{m}_{\text{cyl}}\,\mathrm{d}t = \frac{p_{0,\text{cyl}}M_{0,\text{cyl}}V_{0,\text{cyl}}}{\tilde{R}T_{0,\text{cyl}}} - \int_{t,\text{EVO}}^{t,\text{EVC}}\dot{m}_{\text{cyl}}\,\mathrm{d}t \tag{26}$$

where IVC and IVO are the intake valve closed and open, respectively; and EVC and EVO are the exhaust valve closed and open, respectively. The ideal gas law, Eq. (21), is used in both cases to convert the mass to pressure.

Exhaust and intake terms are used for the valve overlap time:

$$m_{\text{cyl}} = m_{0,\text{cyl}} + \int_{t,\text{IVO,overlap}}^{t,\text{IVC,overlap}}\dot{m}_{\text{cyl}}\,\mathrm{d}t - \int_{t,\text{EVO,overlap}}^{t,\text{EVC,overlap}}\dot{m}_{\text{cyl}}\,\mathrm{d}t \tag{27}$$

The combustion model that is used in the simulation is a heat release model. This model is based on the first law of thermodynamics. One can effectively characterize the combustion process by analyzing either the mass fraction burned $[x_b(\theta)]$ or the gross heat release $[Q_{\text{ch}}(\theta)]$. From theory, the gross heat release rate $(\mathrm{d}Q_{\text{ch}}/\mathrm{d}\theta)$ is

$$\frac{\mathrm{d}Q_{\text{ch}}}{\mathrm{d}\theta} = \frac{\gamma}{\gamma-1}p_{\text{cyl}}\frac{\mathrm{d}V_{\text{cyl}}}{\mathrm{d}\theta} + \frac{1}{\gamma-1}V_{\text{cyl}}\frac{\mathrm{d}p_{\text{cyl}}}{\mathrm{d}\theta} + \frac{\mathrm{d}Q_{\text{ht}}}{\mathrm{d}\theta} \tag{28}$$

Neglecting the effects of convective heat transfer to the cylinder walls, a common approximation can be made, this is the apparent heat release $Q_{\text{app}},(\theta)$, which can be computed directly from pressure–volume $p-V$ data. The apparent heat release rate $\mathrm{d}Q_{\text{app}}/\mathrm{d}\theta$ is expressed as

$$\frac{\mathrm{d}Q_{\text{app}}}{\mathrm{d}\theta}=\frac{\gamma}{\gamma-1}p_{\text{cyl}}\frac{\mathrm{d}V_{\text{cyl}}}{\mathrm{d}\theta}+\frac{1}{\gamma-1}V_{\text{cyl}}\frac{\mathrm{d}p_{\text{cyl}}}{\mathrm{d}\theta} \tag{29}$$

To calculate $\mathrm{d}Q_{\text{app}}/\mathrm{d}\theta$, the cylinder volume must be computed. This can be described by the following function:

$$V_{\text{cyl}}=A_p\{[2a/(r_c-1)]+l+a-a\cos\theta-\sqrt{l^2-a^2\sin^2\theta}\} \tag{30}$$

Differentiating the volume equation with respect to θ, the following function is obtained:

$$\frac{\mathrm{d}V_{\text{cyl}}}{\mathrm{d}\theta}=A_p\left(a\sin\theta+\frac{a^2\sin\theta\cos\theta}{\sqrt{l^2-a^2\sin^2\theta}}\right) \tag{31}$$

Treating γ as a constant, the only term left in the heat-release rate equation is the $\mathrm{d}p_{\text{cyl}}/\mathrm{d}\theta$ term. This is calculated through the numerical differentiation of p_{cyl}. Once $\mathrm{d}Q_{\text{app}}/\mathrm{d}\theta$ is calculated, the apparent heat release $Q_{\text{app}},(\theta)$ can now be calculated through a numerical integration algorithm:

$$Q_{\text{app}}=\int_{\theta_i}^{\theta_f}\frac{\mathrm{d}Q_{\text{app}}}{\mathrm{d}\theta}\,\mathrm{d}\theta \tag{32}$$

We are now in a position to obtain the mass fraction of fuel burned $x_b(\theta)$. The relationship between $Q_{\text{app}},(\theta)$ and the $x_b(\theta)$ is the lower heating value (Q_{lhv}) for the aircraft fuel. This is simply expressed as

$$x_b=\frac{Q_{\text{app}}(\theta)}{Q_{\text{lhv}}} \tag{33}$$

Once $x_b(\theta)$ is obtained, an empirical formula called the Wiebe function is used in conjunction with a nonlinear curve fitting algorithm to find the coefficients to best fit $x_b(\theta)$. The Wiebe function expresses $x_b(\theta)$ in the following empirical fashion:

$$\hat{x}_b=1-\exp\left\{-a_w[(\theta-\theta_0)/\Delta\theta]^{m_w+1}\right\} \tag{34}$$

For the model to be successful, experimental pressure data are needed at the important operating conditions such as idle, take-off, and cruise to calculate the $\%x_b$. Once this has been computed, the Wiebe function coefficients can be calculated using a nonlinear curve-fitting algorithm such as an iterative nonlinear least squares to minimize the cost of a function or

$$\text{Minimize: } f=(x_b-\hat{x}_b)\qquad\text{for}\qquad g(a_w,m_w)=\sum f^2 \tag{35}$$

Now that we have the coefficients a_w and m_w, we plug them into the analytically differentiated mass fraction of fuel burned equation:

$$\frac{\mathrm{d}x_b}{\mathrm{d}\theta}=x_{b,\text{total}}\frac{a_w(m_w+1)}{\Delta\theta}\left(\frac{\theta-\theta_0}{\Delta\theta}\right)^{m_w}\exp\left[-a_w\left(\frac{\theta-\theta_0}{\Delta\theta}\right)^{m_w+1}\right] \tag{36}$$

The $\mathrm{d}Q_{\text{app}}/\mathrm{d}\theta$ equation can be solved for $\mathrm{d}p/\mathrm{d}\theta$. When this is done, we can substitute Eq. (36) to give

$$\frac{\mathrm{d}p_{\text{cyl}}}{\mathrm{d}\theta}=\frac{\gamma-1}{V_{\text{cyl}}}\left[\frac{\mathrm{d}x_b}{\mathrm{d}\theta}Q_{\text{lhv}}\right]-\frac{\gamma}{V_{\text{cyl}}}\frac{\mathrm{d}V_{\text{cyl}}}{\mathrm{d}\theta}p_{\text{cyl}} \tag{37}$$

This equation is then numerically integrated to give the cylinder pressure or the indicated pressure that pushes on the piston head:

$$p_{\text{cyl}}=\int\frac{\mathrm{d}p_{\text{cyl}}}{\mathrm{d}\theta}\,\mathrm{d}\theta \tag{38}$$

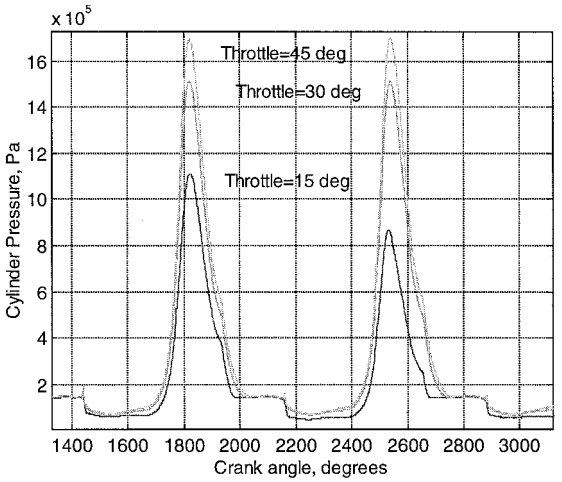

Fig. 5 Simulated cylinder pressure at engine startup.

When collecting the pressure data, it is important to sample at a high resolution to ensure an accurate calculation of the heat-release rate. Sampling rates of every two crank angle degrees have been known to give reasonable accuracy. In addition to knowing the cylinder geometry, spark timing is also an important parameter for combustion analysis. The experimental pressure data were collected from a production automotive engine. This same procedure will be applied to the AVCO Lycoming engine. Figure 5 shows the individual cylinder pressure for three different throttle positions.

Piston Kinematics

The compression ratio is useful because it is often quoted in engine manuals or books, and it can be expressed as

$$r_c=\frac{V_T}{V_c}=\frac{V_d+V_C}{V_c} \tag{39}$$

where V_d can be expressed as

$$V_d=\frac{\pi B_{\text{piston}}^2}{4}L \tag{40}$$

To fully characterize the motion of the piston, and the volume change associated with it, the cylinder volume and its derivative will be restated as

$$V_{\text{cyl}}=A_p\left\{[2a/(r_c-1)]+l+a-a\cos\theta-\sqrt{l^2-a^2\sin^2\theta}\right\} \tag{41}$$

Differentiating the volume equation with respect to θ:

$$\frac{\mathrm{d}V_{\text{cyl}}}{\mathrm{d}\theta}=A_p\left(a\sin\theta+\frac{a^2\sin\theta\cos\theta}{\sqrt{l^2-a^2\sin^2\theta}}\right) \tag{42}$$

Torque Production and Friction Model

Many forces act on a piston inside the cylinder chamber. These forces generate torque on the crankshaft. The force that is a direct result of the cylinder pressure or indicated pressure P_{cyl} generates the positive work done by the engine on the piston crown. Through the use of geometric relationships of the piston assembly, we can characterize the indicated torque as

$$T_i=(P_{\text{cyl}}-P_{\text{crank}})A_p a f_1(\theta) \tag{43}$$

$$f_1(\theta)=\sin\theta\left[1+\frac{\lambda_{\text{crank}}\cos\theta}{\sqrt{1-(\lambda_{\text{crank}}\sin\theta)^2}}\right] \tag{44}$$

The reciprocating torque that is generated by the rotation of an equivalent mass can be described as

$$T_r=M_{\text{eq}}a^2 f_1(\theta)\left[f_1(\theta)\ddot{\theta}+f_2(\theta)\dot{\theta}^2\right] \tag{45}$$

$$f_2(\theta) = \frac{\lambda_{\text{crank}} \cos 2\theta}{\sqrt{1-(\lambda_{\text{crank}} \sin\theta)^2}} + \frac{\lambda_{\text{crank}}^3 (\sin 2\theta)^2}{4\sqrt{\left[1-(\lambda_{\text{crank}} \sin\theta)^2\right]^3}} + \cos\theta \tag{46}$$

The friction torque used from Ref. 10 is given by

$$T_f = c_1\dot{\theta} + c_2 P_{\text{cyl}} \mu_f |f_1(\theta)| \tag{47}$$

Expressing the oil viscosity as a function of temperature:

$$\mu_f = 6.31 \log^{-1}\left\{-5 + 4.54[1 + (T_{\text{oil}}/135)]^{-1.3}\right\} \tag{48}$$

The three torques can be summed to get the net torque. The overall torque T_{cyl} can thus be expressed as

$$T_{\text{cyl}} = T_i - T_r - T_f \tag{49}$$

This overall torque generated from the piston is only one torque acting on the crankshaft. For a four-cylinder configuration, individual cylinder pulses will result from the torque generated by each cylinder. The individual cylinder torques coupled with the torque generated by the propeller system will form a basis for the crankshaft dynamics.

Crankshaft Dynamics

The crankshaft can be modeled to many different levels of complexity. A simple model is to assume that the entire crankshaft is lumped into a single inertia and a single damping coefficient. For GA aircraft engines, this is not a bad assumption because the crankshaft tends to be short due to the horizontally opposed piston arrangement and close proximity of the propeller. The inertia in this case is considered to be a sum of the engine and propeller inertias.

Applying Newton's second law we have

$$\sum_{i=1}^{\text{numcyl}} T_{\text{cyl},i} - T_{\text{load}} - B\omega = J\dot{\omega} \tag{50}$$

Converting the equation from the time domain to the crank angle domain we get the following equation:

$$\frac{\mathrm{d}\omega}{\mathrm{d}\theta} = \frac{\sum_{i=1}^{\text{numcyl}} T_{\text{cyl},i} - T_{\text{prop}}}{J\omega} - \frac{B}{J} \tag{51}$$

Integrating this equation in the crank angle domain gives the engine speed for the aircraft engine.

Exhaust Modeling

Because the exhaust manifold is nearly identical to the intake manifold, the exact same form will be used here. This means that the equation is as follows:

$$\frac{\mathrm{d}m_{a,\text{ex}}}{\mathrm{d}t} = \sum_{i=1}^{\text{numcyl}} \dot{m}_{\text{cyl},i} - \dot{m}_{\text{out}} \tag{52}$$

The time delay for the exhaust gas to reach the EGO sensor can be expressed as

$$\Delta t = R_l p_{\text{ex}} A_{\text{run}} / R T_{\text{ex}} \dot{m}_{\text{out}} \tag{53}$$

Simulation and Experimental Results

Several maneuvers have been attempted to validate the data for a Lycoming IO-360 engine. The Lycoming IO-360 is a four-cylinder engine with horizontally opposed pistons, natural aspiration (no turbocharging or supercharging), and continuous-flow fuel injection. Some of the IO-360 engine specifications are shown in Table 1.

Validation data were supplied from a test cell in the Engine Research Center at West Virginia University for three test runs. These test runs represent frequently used operating conditions for the engine. A large flywheel is used to replace the propeller inertia.

Figures 6–13 represent the transient responses in simulated and experimental runs. Figures 6–9 show results for test-1, which represents a throttle step change from 20 to ~36%. Figures 10–13 show results for test-2, which represents a throttle step of 89–24%. Figure 6 shows the response in the engine speed. The action of the closed-loop controller in maintaining a steady-state speed of 2700 rpm is apparent. The manifold pressure response (Fig. 7) shows increasing manifold pressure, as expected. Figure 8 shows the torque response to a step increase in throttle. This response can be explained by noting that for a fixed rpm, the dynamometer is controlling rpm to absorb the torque output of the engine. Figure 9 shows the air–fuel ratio response; some deviation between the simulation response

Table 1 Lycoming IO-360 engine parameters

Physical parameter	Value	Units
Compression ratio	8.5	——
Bore	0.1302	m
Stroke	0.1111	m
Displacement	0.0059	m^3
Piston area	0.0133	m^2
Crank radius	0.0556	m
Connecting rod length	0.1710	m
Engine/flywheel inertia	0.0360/1.0142	Nms^2
Equivalent reciprocating mass	1.26	kg

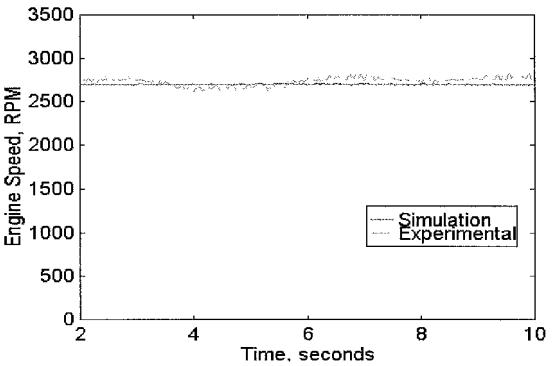

Fig. 6 Engine speed for a step transient test no. 1.

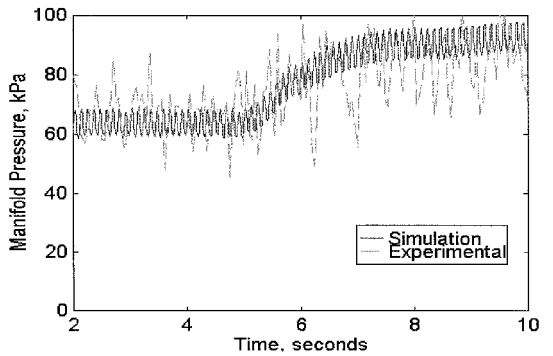

Fig. 7 Manifold pressure for a step transient test no. 1.

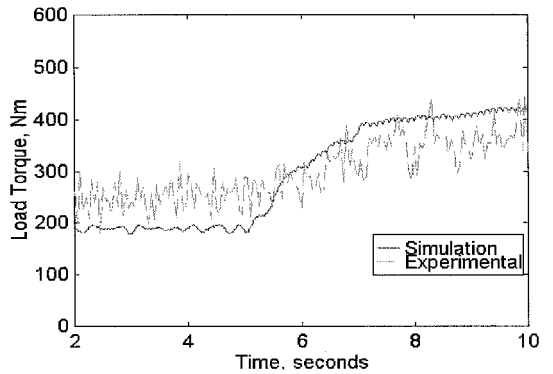

Fig. 8 Load torque for a step transient test no. 1.

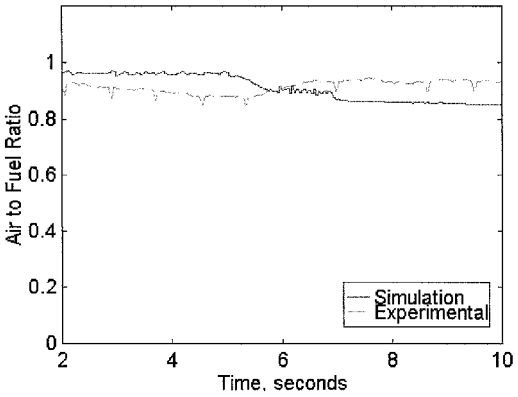

Fig. 9 Air-to-fuel ratio for a step transient test no. 1.

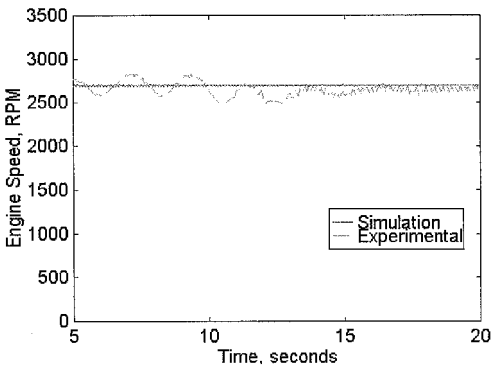

Fig. 10 Engine speed for a step transient test no. 2.

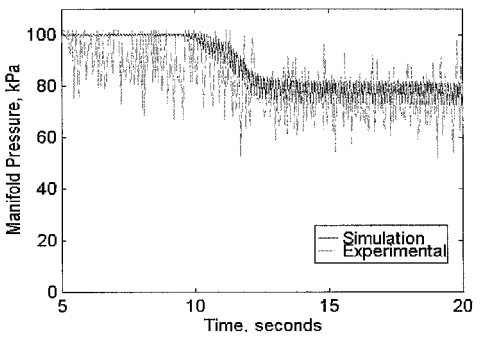

Fig. 11 Manifold pressure for a step transient test no. 2.

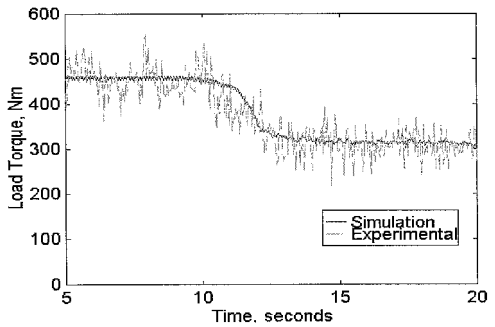

Fig. 12 Load torque for a step transient test no. 2.

and experimental results is apparent. As mentioned earlier, a number of parameters necessary for validating the simulation were not available; hence, a number of approximations had to be introduced. For example, the in-cylinder pressure data that are essential for the combustion model were not available for the IO-360 engine. Hence, pressure data from an automotive engine was used instead. The second set of figures shows the response to stepdown in the throttle from 89 to 24%. This is a large step that tests the simulation. Figure 10 shows that the rpm remains fixed due to the closed-loop control of the engine speed. Figure 11 shows the drop in manifold pressure

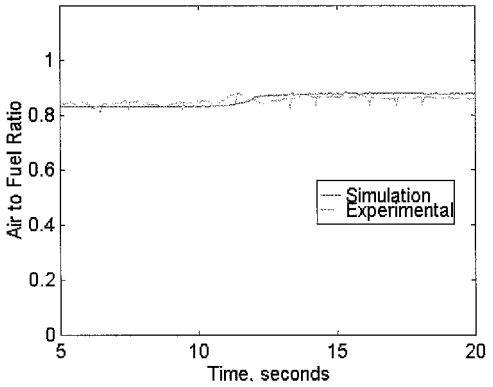

Fig. 13 Air-to-fuel ratio for a step transient test no. 2.

when the stepdown to 24% occurs. Figure 12 shows the torque reduction while the speed is maintained at 2700 rpm. Figure 13 shows the air–fuel ratio for the stepdown in throttle.

Conclusions

The model was assembled and partially validated for a Lycoming IO-360 engine. The individual cylinder model performs well with the given level of sophistication of the cylinder pressure and combustion models. The individual cylinder simulation tracks the experimental data well for the higher throttle angles (13% and up). One reason for this is the modeling of combustion in the crank angle domain. The discrepancy between experimental and theoretical results is within 10% for throttle positions greater than 13%.

A feature to be noted in the simulation results is the presence of oscillations. This is easily explained if one realizes that the simulation is an inherently less-damped system compared with a real engine. These results were produced using real-time data as input to the simulation, the influence of which cannot be ruled out. We draw attention to the fact once again that in the absence of in-cylinder pressure data from the IO-360 engine, pressure data from an automotive engine were used. These are reasonable results for the given validation data set. To obtain more accurate simulation results, detailed experimental data are needed for system identification purposes. Currently work on the simulation is being continued under sponsorship from NASA. In the very near future, a complete data set representative of the IO-360 engine is to be collected with the aircraft in flight. It is believed that this will greatly enhance the accuracy of this simulator.

This model is currently being used to develop alternate control strategies for implementation of a single-lever operation. Various schemes incorporating advanced sensor and actuator technology for improved performance are being researched. Strategies such as turbocharging, EGR, spark, and fuel control will be studied with a view to not only improving performance but also tackling issues such as emissions.

Fault detection of aircraft sensors and actuators is another area that can be studied using this simulator. This could lead to the integration of diagnostics and control, making the overall control strategy more fault tolerant.

Acknowledgments

We gratefully acknowledge the support provided for this work by NASA under the AGATE program, Grant NCA3-AGATE-122; and West Virginia University and Lycoming through access to experimental data.

References

[1]Richard, J. C., "Low-Order Nonlinear Dynamic Model of IC Engine-Variable Pitch Propeller System for General Aviation Aircraft," NASA TM 107006, July 1995.

[2]Rizzoni, G., Parker, G., and Dawson, J., "Individual Cylinder Model of IC Engine-Variable Pitch Propeller System for GA Aircraft," Ohio State Univ. Powertrain Control and Diagnostics Lab., Rept. 733726-9602, Nov. 1996.

[3]Rizzoni, G., "ME 781 Powertrain Dynamics Class Notes," Dept. of

Mechanical Engineering, Ohio State Univ. Columbus, OH, 1996.

[4]Kao, M., and Moskwa, J. J., "Turbocharged Diesel Engine Modeling for Nonlinear Engine Control and State Estimation," *Advanced Automotive Technologies*, DSC-Vol. 52, American Society of Mechanical Engineers, New York, 1993, pp. 135–146.

[5]Kao, M., and Moskwa, J. J., "Turbocharged Diesel Engine Modeling for Nonlinear Engine Control and State Estimation," *Journal of Dynamic Systems, Measurements, and Control*, Vol. 117, No. 1, 1995, pp. 20–30.

[6]Dobner, D. J., "A Mathematical Engine Model for Development of Dynamic Engine Control," Society of Automotive Engineers, TP 800054, Feb. 1980.

[7]Cook, J. A., and Powell, B. K., "Discrete Simplified External Linearization and Analytical Comparison of IC Engine Families," *Proceedings of the American Control Conference*, Vol. 1, 1987, pp. 326–331.

[8]Moskwa, J. J., and Hedrick, J. K., "Modeling and Validation of Automotive Engines for Control Algorithm Development," *Advanced Automotive Technologies*, American Society of Mechanical Engineers, DSC-Vol. 13, New York, 1989, pp. 237–247.

[9]Cook, J. A., and Powell, B. K., "Modeling of an Internal Combustion Engine for Control Analysis," *IEEE Control Systems Magazine*, Aug. 1988, pp. 20–25.

[10]Ciulli, E., Rizzoni, G., and Dawson, J., "Numerical and Experimental Study of Friction on a Single Cylinder CFR Engine," Society of Automotive Engineers, TP 960357, Feb. 1996.

[11]Von Misses, R., *Theory of Flight*, Dover, New York, 1959.

[12]Fox, R. N., and McDonald, A. T., *The Fundamentals of Fluid Dynamics*, Wiley, New York, 1992.

[13]Heywood, J. R., *Internal Combustion Engine Fundamentals*, McGraw–Hill, New York, 1988.

[14]Aquino, C. F., "Transient A/F Control Characteristics of the 5 Liter Central Fuel Injection Engine," Society of Automotive Engineers, TP 810494, 1981.

[15]Dawson, J. A., "An Experimental and Computational Study of Internal Combustion Engine Modeling for Controls Oriented Research," Ph.D. Dissertation, Dept. of Mechanical Engineering, Ohio State Univ., Columbus, OH, 1996.